Dendrimer Stabilized Nanoalloys for Ink-Jet Printing of Surface-Enhanced Raman Scattering Substrates

Tiago Fernandes[a], Natércia C. T. Martins[a], Sara Fateixa[a], Helena I. S. Nogueira[a], Ana L. Daniel-da-Silva[a], Tito Trindade[a]*

[a]Department of Chemistry, CICECO- Aveiro Institute of Materials, University of Aveiro, 3810-193 Aveiro, Portugal

Abstract

Research on paper substrates prepared by inkjet deposition of metal nanoparticles for sensing applications has become a hot topic in recent years; however, the design of such substrates based on the deposition of alloy nanoparticles remains less explored. Herein, we report for the first time the inkjet printing of dendrimer-stabilized colloidal metal nanoalloys for the preparation of paper substrates for Surface-enhanced Raman scattering (SERS) spectroscopy. To this end, nanoassemblies containing variable molar ratios of Au:Ag were prepared in the presence of poly(amidoamine) dendrimer (PAMAM), resulting in plasmonic properties that depend on the chemical composition of the final materials. The dendrimer-stabilized Au:Ag:PAMAM colloids exhibit high colloidal stability, making them suitable for the preparation of inks for long-term use in inkjet printing of paper substrates. Moreover, the pre-treatment of paper with a polystyrene (PS) aqueous emulsion resulted in hydrophobic substrates with improved SERS sensitivity, as illustrated in the analytical detection of tetramethylthiuram disulfide (thiram pesticide) dissolved in aqueous solutions. We suggest that the interactions established between the two polymers (PAMAM and PS) in an interface region over the cellulosic fibres, resulted in more exposed metallic surfaces for the adsorption of the analyte molecules. The resulting hydrophobic substrates show long-term plasmonic stability with high SERS signal retention for at least ninety days.

Keywords: Dendrimers, metal nanoalloys, paper sensors, SERS.

Graphical abstract

Paper-based substrates containing dendrimer-stabilized Au:Ag:PAMAM nanoalloys for the SERS probing of the pesticide thiram in an aqueous solution.

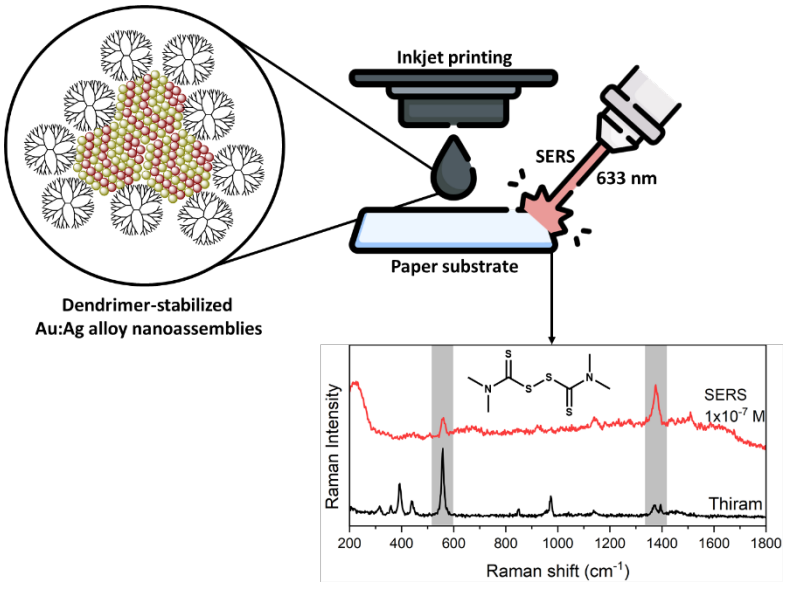

1. Introduction

In the past decade, inkjet printing has been investigated as an attractive method for the design of versatile and easy-to-use sensors[1, 2]. Indeed, the inkjet deposition of colloidal nanoparticles provides a low-cost and straightforward approach delivering additional properties onto a substrate, such as plasmonic properties[3-5], conductivity[6-8] or catalytic activity[9]. This printing technique is also versatile concerning the types of substrates employed, for example by allowing the deposition of nanopatterned structures using standard office paper with refillable cartridges[10] and the large-scale fabrication of sensors of varying chemical composition on different types of materials (*e.g.,* cellulose fibres, silicon wafers or glass surfaces)[11-16]. In particular, the paper is highly attractive to develop sensing platforms since it offers several advantages such as flexibility, portability, low cost and recyclability[17, 18].

Surface-enhanced Raman scattering (SERS) spectroscopy is a powerful technique for molecular screening in several fields such as environmental analysis, food safety, biomedicine, and others[19-21]. The SERS technique delivers several advantages such as the ability to probe very low concentrations of several target analytes while being a non-destructive method that requires small samples volumes with minimal sample treatment[22-25]. The SERS effect relies on the strong intensification of the Raman signal of molecules adsorbed or in the vicinity of metal surfaces with localized surface plasmon resonances (LSPR), resulting in the enhancement of the local electric field (an electromagnetic mechanism) or charge transfer due to metal-adsorbate complex formation (a chemical mechanism). The Raman signal enhancement is higher on plasmonic structures that display nanogaps or on the apex features of anisotropic plasmonic particles, where analytes can adsorb; such regions of an enhanced local electric field are commonly referred to as hotspots. Consequently, the design of substrates based on these materials with high efficiency, reproducibility and stability is of upmost importance for using SERS as a molecular screening technique. Moreover, with the advent of portable Raman spectrometers, the design of lightweight and streamlined substrates becomes increasingly important for on-site analysis[26, 27]. In this context, the development of flexible SERS substrates produced by inkjet printing has been steadily increasing in recent years[1, 28, 29].

Most of the reported SERS substrates prepared by inkjet printing involve platforms containing Au or Ag nanoparticles allowing the detection of a wide variety of analytes dispersed on different matrices[30-33]. These platforms are either prepared by printing pre-synthesized metal

nanoparticles on a solid substrate[34] or by *in situ* synthesis of the nanoparticles on the substrate surface after inkjet printing metal salts and reducing agents[35]. Ink additives or additional substrate treatments may be employed to further improve the functionality of the resulting material. The inkjet printing of SERS substrates using plasmonic metal alloys has been scarcely reported, despite some reports demonstrating superior performance in certain situations. Hence, Weng et al. reported the preparation of inkjet-printed Au nanoparticle paper substrates with enhanced SERS activity and reproducibility, by growing a second metal (silver) phase [36]. In brief, the Au seeds were deposited on filter paper using a conventional inkjet printer and then, the Ag nanoparticles were grown *in situ* by submerging the paper substrates in a solution containing the Ag(I) precursor and reducing agents. The authors were able to control the reaction conditions regarding the degree of Ag deposition to produce SERS substrates that display superior performance when compared with bare Au NPs on paper.

Several limitations have been attributed to the use of colloidal suspensions for inkjet deposition, especially regarding the tendency of particulates to clog the ejection nozzle due to deposition on printhead surfaces[37]. The formulation of inks with long term colloidal stability and tuned particle size distribution is a crucial processing requirement, which might explain to some extent the lack of studies using colloidal metal nanoalloys for inkjet printing. To overcome these disadvantages, we have explored the synthesis of dendrimer-stabilized metal nanoassemblies, where the dendrimers are known for their well-defined architecture and whose terminal chemical groups account for efficient capping and colloidal stabilization of metal nanoparticles[38, 39]. Moreover, the tuneable surface chemistry of dendrimers can be explored to promote chemical functionalization or entrap analytes of interest[39]. Among the extensive library of dendritic molecules, we have selected PAMAM dendrimers for the synthesis of metal nanoparticles, given their well-established physicochemical properties and commercial availability[40, 41]. Furthermore, PAMAM dendrimers offer several advantages for the preparation of colloids for inkjet printing. In fact, the high density of functional groups of the 5^{th} generation PAMAM dendrimers delivers important multivalency, which is an essential feature for long-term colloidal stability and posterior robust interaction of the nanoalloys on the paper substrates. Moreover, the relatively monodisperse molecular weight distribution, nanosize and globular shape of PAMAM dendrimers in solution, provides a way to prepare inks with consistent and reliable proprieties (*i.e.* viscosity or jetting characteristics) when compared with linear polymers of equivalent molecular weight[42].

Recently, our group reported a one-step method for the fabrication of hydrophobic paper-based substrates by the deposition of Ag nanoparticles and polystyrene beads. The resulting substrates displayed good SERS performance for the detection of thiram spiked in several matrices, such as mineral water, orange juice or apple peel[34]. In this work, we wish to report for the first time the use of dendrimer-stabilized Au:Ag nanoalloys of variable molar ratios, as colloidal stable inks for the inkjet deposition on common office paper. The resulting substrates were then investigated regarding their SERS sensitivity using thiram as a model pesticide. To further improve the SERS performance of the resulting substrates, the paper surface was pre-treated with a hydrophobic coating of polystyrene (Scheme 1). The substrates reported in this work provide an innovative strategy for the design of paper-based Au:Ag:PAMAM nanoassemblies for SERS detection of analytes dissolved in water samples.

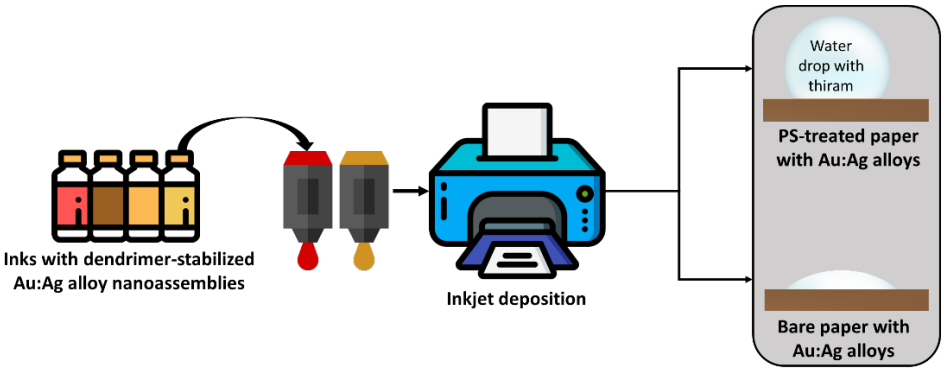

Scheme 1 – Colloids of dendrimer-stabilized Au:Ag nanoalloys in inks formulations for the preparation of paper-based SERS substrates, with and without pre-treatment using polystyrene (PS).

2. Experimental section

2.1. Materials

All chemicals were used without any further treatment: G5-NH_2 PAMAM dendrimers (Dendritech, Midland, MI, USA); Tetrachloroauric(III) acid trihydrate ($HAuCl_4 \cdot 3H_2O$, 99.9%, Sigma-Aldrich); Silver nitrate ($AgNO_3$, Sigma-Aldrich, >99.0%); sodium dodecyl sulfate salt (SDS, $NaC_{12}H_{25}SO_4$, Sigma-Aldrich, >98.0%); α,α'-azobis-(isobutyronitrile) (AIBN, $C_8H_{12}N_4$, Fluka >98.0%); hexadecane ($C_{16}H_{34}$, Sigma-Aldrich, >99.0%), glycerol ($C_3H_8O_3$, Sigma-Aldrich, >99.0%); sodium bicarbonate ($NaHCO_3$, Sigma-Aldrich, >99.5%) Thiram ($C_6H_{12}N_2S_4$, Sigma-Aldrich, ≥98.0%); Styrene (C_8H_8, Aldrich 99%) was purified over a column of neutral Al_2O_3 and stored at 4 °C. Colloids of gold, silver and their alloys were prepared using ultrapure water (18.2 MΩ·cm,

25 °C, MilliQ, Millipore); A4 office paper sheets with a grammage of 80 g m^{-2} (Navigator, Portugal) were used for the preparation of the SERS substrates.

2.2. Synthesis of dendrimer-stabilized Au:Ag alloy nanoassemblies

The dendrimer-stabilized Au:Ag nanoassemblies were prepared according to the procedure previously reported by our group[43]. Typically, 60 mg of PAMAM dendrimer was added to 10 mL of ultrapure water and left to disperse under vigorous stirring (750 rpm) for 15 minutes. Then, various proportions of the Ag(I) and Au(III) salts were added to obtain the alloy nanoparticles by keeping as 20:1 the concentration ratio of metal to the dendrimer. For example, for the particles with the 10:10:1 molar ratio (Au:Ag:PAMAM), 100 µL of aqueous $AgNO_3$ (227.3 mM) and 900 µL of aqueous $HAuCl_4 \cdot 3H_2O$ (25.4 mM) were mixed. The reaction was then left to proceed for 24 hours at 25 °C. Throughout the reaction, it was observed a gradual change in colour for all the systems. The molar ratios of 15:5:1, 10:10:1 and 5:15:1 Au:Ag:PAMAM were used for preparing the nanoalloys described in this work. Monometallic particles of Au (20:0:1) and Ag (0:20:1) were also prepared for comparative purposes. The procedure to prepare these particles was similar to the described for the alloys, but in this case, the temperature and reaction time were 60 °C and 3 hours, respectively. The nominal molar ratio of the Au:Ag dendrimer-stabilized nanoassemblies, which were named Au:Ag:PAMAM, will be indicated in the text by the distinct values of Au:Ag ratio, since for PAMAM the respective value was 1 in all the inks.

2.3. Synthesis of polystyrene emulsions

The polystyrene (PS) emulsions were prepared by following the procedure previously reported by our group with some modifications[34, 44]. Briefly, the monomer styrene (0.032 mol), hexadecane (3.31×10^{-4} mol) and the initiator α,α'-azobis-(isobutyronitrile) (AIBN, 1.28×10^{-4} mol) were mixed with an aqueous solution of sodium dodecyl sulfate (SDS, 2×10^{-4} mol) and sodium bicarbonate ($NaHCO_3$, 1.73×10^{-4} mol). This mixture was then kept under vigorous magnetic stirring for 30 min followed by sonication (amplitude 35%, 20 W power, Sonics-Vibracel Sonifier) for 7 minutes. The resulting miniemulsion was then transferred to a "jacket" glass reactor with mechanical stirring (500 rpm) and nitrogen (N_2) inlet. The reactor content was deoxygenated by purging with N_2 for 20 min.,and then the temperature of the miniemulsion was set to 70 °C using a thermostatic bath. The polymerization reaction was allowed to proceed for 4 hours under N_2 atmosphere, 500 rpm.

2.4. Inkjet printing of SERS substrates

To prepare inks suitable for printing, the Au, Ag and alloy dendrimer-stabilized nanoassemblies were mixed with glycerol to adjust the viscosity to an optimum level for inkjet printing (2-3 cP)[34]. Typically, 7.2 ml of each colloid were mixed with 1.8 ml of glycerol under magnetic stirring for 15 min. After adding glycerol, no significant changes were observed in the colloidal stability of the nanoparticles, except for the monometallic dendrimer-stabilized Ag nanoparticles where a slight colour change was observed (from brown to dark brown). In this case, the solution was left for 24 hours after mixing with glycerol and no further visual changes were observed thereafter, which may be explained by the reduction of non-reacted Ag(I) after adding glycerol[45].

For the more concentrated inks, the dendrimer-stabilized nanoparticles were firstly lyophilized (Au:Ag, 4.5 mM nominal concentration) and then redispersed in half the volume of water (Au:Ag, 9 mM nominal concentration). The resulting colloid was then used for the preparation of an ink following a similar procedure, as described above.

The colloidal inks were transferred to refillable ink cartridges and were used to print the SERS substrates (0.5 cm x 0.5 cm) on office paper using a piezoelectric printer (Epson Expression Home XP-255). The substrates were prepared after 10, 15 and 20 printing cycles, to increase the local concentration of nanoparticles in the paper. To confer hydrophobic characteristics to the substrate, the paper surface was pre-treated with a polystyrene emulsion (0.6% w/v, 15 printing cycles) and only then ink-jet printing of the metal colloids was performed.

2.5. SERS measurements and Raman imaging

The SERS analyses of aqueous solutions of thiram were carried out by the deposition of an aliquot (≈ 10 µL) of the sample solution on each paper substrate and left to dry at 40 °C. The sample solutions were prepared by the required dilution in ultra-pure water of a thiram stock solution ($1x10^{-3}$ M) in methanol. For SERS experiments, thiram was selected a model probing molecule since it is one of the simplest dithiocarbamate pesticides with well-established chemistry regarding its interaction with Ag/Au surfaces. It is also convenient for comparative purposes with other research works on the development of SERS substrates for pesticide monitoring.

The sensitivity and homogeneity of the substrates were assessed by high-resolution Raman imaging by obtaining 150 x 150 Raman spectra (total of 22 500 spectra) in an area of 30 x 30 µm with an acquisition time of 0.1 s. The images were built by the integration of the absolute area of the thiram diagnosis band located at 1374 cm^{-1}. To compare the SERS sensitivity between different substrates, 50 spectra were extracted from the brighter yellow areas of the Raman

192 map (areas where thiram is adsorbed to the metal resulting in the strongest SERS signal of the
193 chosen band) of each substrate, and an average Raman spectrum was obtained using WITec
194 software Project 5^+. The signal-to-noise ratio (SNR) was determined by calculating the average
195 peak height of the typical SERS band (S) from two independent spectra, divided by the square
196 root of the standard deviation of the peak height (σ_y)[46].

197 **2.6. Instrumentation**

198 The UV/VIS spectra were recorded using a GBC Cintra 303 UV/Visible spectrophotometer. For
199 the paper substrates, the optical spectra were recorded in the diffuse reflectance mode using
200 MgO as reference and converted to absorbance spectra. The scanning electron microscopy
201 (SEM) micrographs were obtained using the Hitachi SU-70 with operating voltage at 4 kV. High-
202 resolution transmission electron microscopy (TEM) micrographs of the colloids were acquired
203 using the JEOL 2200FS HR-TEM. Energy-dispersive X-ray spectroscopy (EDS) studies were
204 performed using Bruker Esprit. Samples for TEM and EDS were prepared by diluting the original
205 colloids and depositing them on a carbon-coated Cu grid. Dynamic light scattering (DLS) and zeta
206 potential measurements were accomplished using a Malvern Zetasizer Nano ZS equipped with
207 a standard 633 nm laser. Raman and atomic force microscopy (AFM) studies were accomplished
208 using a combined Raman-AFM-SNOM confocal microscope WITec alpha300 RAS+. For the
209 Raman studies, a He:Ne laser operating at 633 nm was used as the excitation source with power
210 set at 1.5 mW. The AFM measurements were carried out in tapping mode (AC-AFM) using a
211 tip-cantilever silicon reflex-coated with a spring constant of k = 2.8 N/m and 75 kHz of resonance
212 frequency. The scanning image was 1 µm × 1 µm (256 points per line × 256 lines per image) with
213 a scan speed of 1 s/line (the same retrace speed). The static water contact angle (WCA)
214 measurements were performed using an OCA 20 goniometer (DataPhysics Instruments GmbH)
215 by placing an ultrapure water droplet of 3 µL onto the paper substrates. The values of the
216 contact angles presented in this work are the average of at least three measurements. The
217 inductively coupled plasma - optical emission spectroscopy (ICP-OES) analysis was carried out
218 using a Jobin Yvon Activa M equipment.

219

220 **3. Results and discussion**

221 **3.1. Inkjet printing of Au:Ag:PAMAM paper substrates**

222 In this work, we have prepared colloids of Au:Ag:PAMAM nanoalloys of raspberry-like particles
223 with an average size ranging from 80 to 200 nm, following a methodology previously reported

by us (Figures 1 and S1 supporting information)[43]. For comparative purposes, the corresponding dendrimer-stabilized monometallic nanoparticles based only on Ag or Au were also prepared (Figure S2). The ensuing metal colloids display a positive surface charge (> 60 mV) at pH 7, as previously determined by zeta potential measurements, which accounts for the presence of the PAMAM dendrimer as capping agent[43].

Figure 2 shows the UV/VIS spectra of office paper printed with the monometallic and alloyed dendrimer-stabilized Au:Ag:PAMAM nanoparticles. For comparative purposes, the optical spectra of the original colloids are also shown. The monometallic Au and Ag colloids show a well-defined band peaked at 520 and 415 nm, respectively, corresponding to the LSPR of the respective nanometals. Instead, the optical spectra of the colloidal nanoassemblies display broader LSPR bands in the region 400-520 nm, which might indicate interparticle plasmon coupling. As a general trend, the UV/VIS spectra of the paper substrates show strong band broadening and a redshift on the absorption maximum, which we attribute to the presence of a distinct dielectric (cellulose), though particles' clustering can also contribute to such observations.

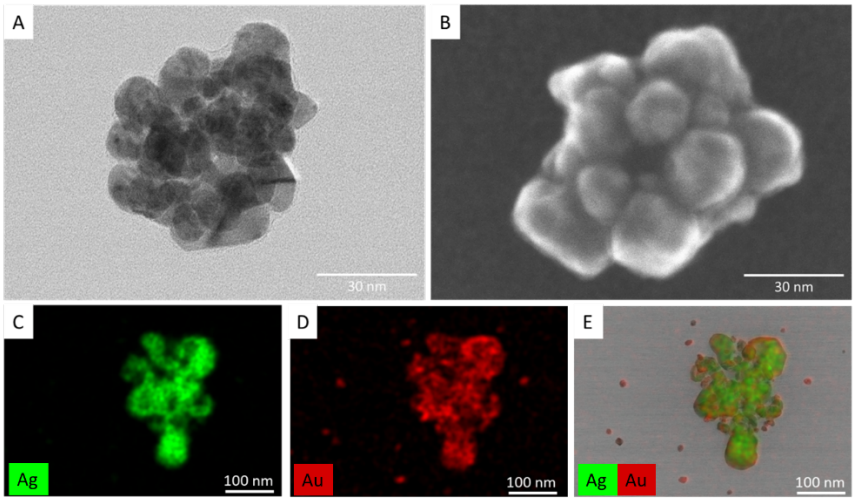

Figure 1 – Transmission electron microscopy (TEM) and scanning electron microscopy (SEM) images of 15:5 Au:Ag dendrimer-stabilized nanoassemblies with raspberry-like structure (A,B); EDS mapping of 5:15 Au:Ag dendrimer (PAMAM)-stabilized nanoassemblies (C-E).

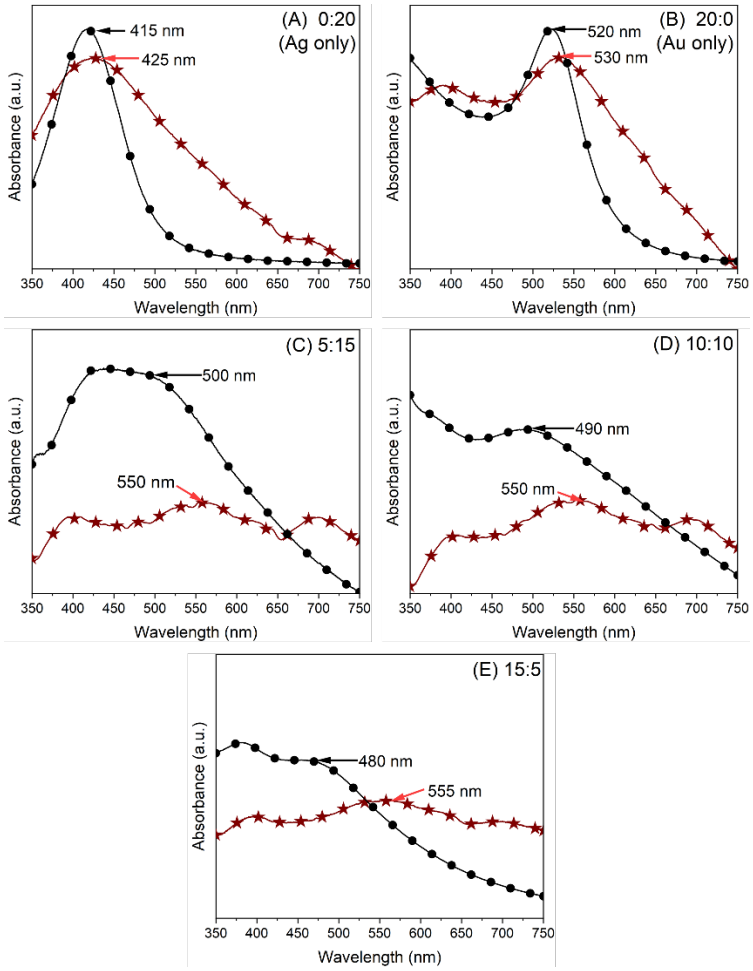

Figure 2 – UV/VIS spectra of paper substrates after 20 printing cycles of inks containing PAMAM-stabilized nanoparticles with variable Au:Ag molar ratios, as indicated (–★–). For comparative purposes, the UV/VIS spectra of the respective aqueous colloids are also shown (—●—).

After inkjet printing on paper substrates, all samples were analysed by SEM to inquire about the distribution and morphology of the dendrimer-stabilized nanoalloys over the cellulose fibres. Figure 3 (and Figures S3-S4) show the SEM micrographs for the substrates analysed, in which the raspberry-like morphologies are observed as particulates dispersed over the cellulose fibres. For comparison, SEM micrographs of the bare office paper are also presented in Figure S5 (supporting information). Note that the bare office paper contains micron-sized particulates over the cellulose fibres due to the presence of mineral fillers (e.g. $CaCO_3$), which are used in the papermaking process[47]. The SEM micrographs of the inkjet-printed substrates with the monometallic nanoparticles display the similar size and morphology of the colloidal particles previously analysed by TEM (Figure S2, supporting information). On the substrates with the 20:0 Au:Ag:PAMAM nanoparticles, many individualized nanoparticles (≈20 nm) are dispersed along the cellulose fibres, with the presence of small agglomerates that typically appear due to the inkjet deposition. On the other hand, the substrates with 0:20 Au:Ag:PAMAM nanoparticles

display a polydispersed size distribution where smaller nanoparticles (≈20 nm) are surrounding bigger individual particles (≈ 200 nm). The conjugate effect of using PAMAM dendrimer as the only reducing agent and the lower reduction potential of Ag(I) may explain the polydispersity observed for the monometallic Ag nanoparticles[43]. While the monometallic nanoparticles are individualized, the alloy nanoparticles are organized in assemblies that are held together by the dendrimer, resulting in bigger and raspberry-like structures (Figures 1 and S1, supporting information)[43]. The SEM images of the paper substrates (Figure 3 and Figure S4) with the alloy nanoparticles display the typical nanoassemblies (≈80-200 nm) dispersed along the cellulose fibres that are analogous in size and shape to the ones observed in the colloidal form (Figures 1 and S1, supporting information). In addition, the metal content (Au:Ag) measured for each paper substrate by ICP-OES is in fair agreement with the expected nominal values (Table S1).

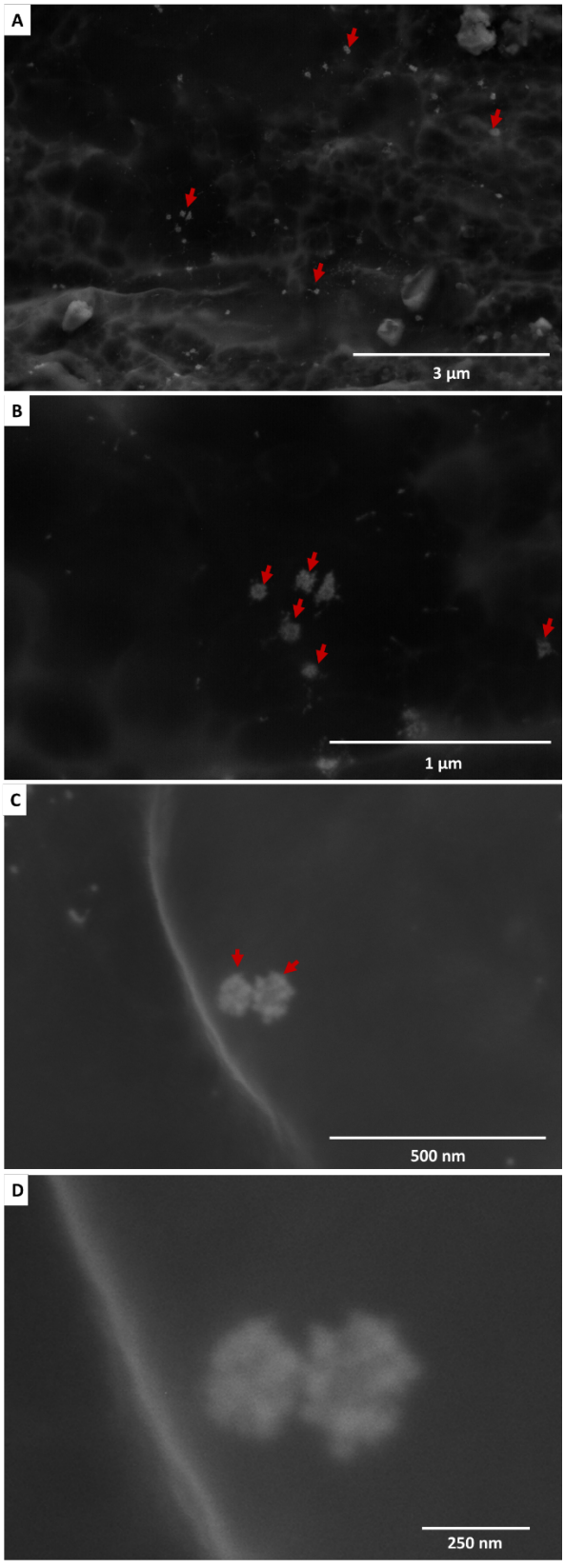

Figure 3 – SEM micrographs of a paper substrate after 20 printing cycles using ink 15:5 Au:Ag:PAMAM (A-C: red arrows indicate the raspberry-like nanoassemblies; D is the zoomed-in image of C; A-B, back-scattered electron (BSE) mode; C, secondary electron (SE) mode).

3.2. SERS studies using inkjet printed paper substrates

3.2.1. Paper substrates containing Au:Ag PAMAM-stabilized nanoassemblies

The SERS performance of the paper substrates was assessed after inkjet printing either the colloids of dendrimer-stabilized monometals or the nanoalloys. Figure 4 shows the SERS spectra of thiram, which was used as a model pesticide, using a series of paper substrates obtained after 20 printing cycles.

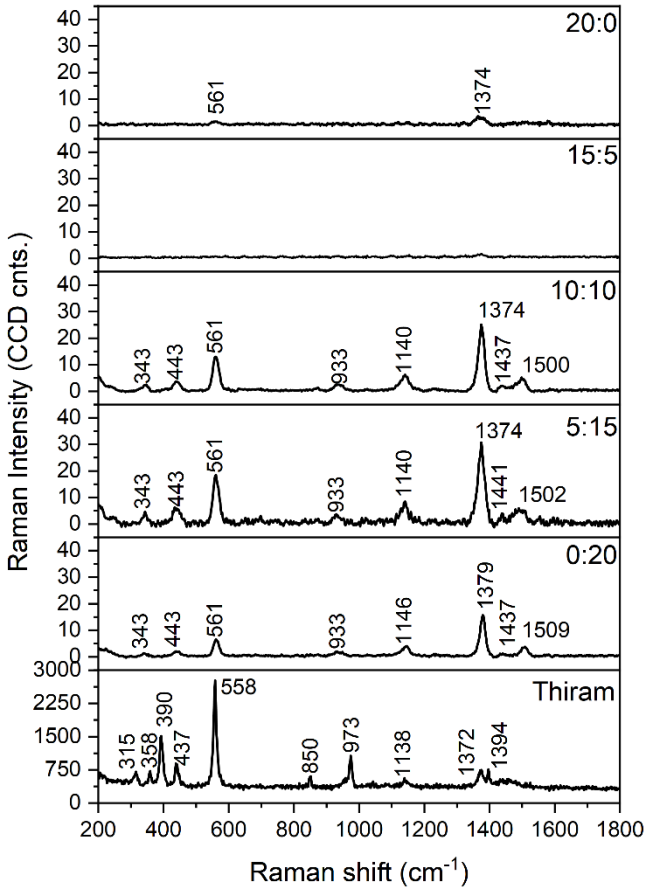

Figure 4 – SERS spectra of thiram ($1x10^{-4}$ M in the sample solution) collected on paper substrates printed with inks having the indicated Au:Ag molar ratio in the PAMAM-stabilized nanoassemblies. All the SERS spectra were built by extracting the most intense 50 data points from the respective Raman images. For comparative purposes, the conventional Raman spectrum of thiram powder is also presented.

The inkjet 5:15 Au:Ag:PAMAM printed paper was used as the SERS substrate for assigning the vibrational bands of thiram (Figure 4), as follows[48-50]: 343 cm^{-1} ν(Ag-S); 443 cm^{-1}, δ(CSS) and δ(CNC); 561 cm^{-1}, ν_{sym}(CSS) coupled to ν(S-S); 933 cm^{-1} ν(C-S); 1140 cm^{-1}, ρ(CH_3)+ν(N–CH_3); 1374 cm^{-1} δ_{sym}(CH_3); 1441 cm^{-1} δ_{asym}(CH_3); 1502 cm^{-1} ν(CN). Figure 4 indicates that the best SERS performance was observed for inks containing dendrimer-stabilized Au:Ag nanoalloys with

metal ratios 5:15 and 10:10. In fact, in these substrates, there is a strong enhancement of the Raman signal as clearly observed in the band at 1374 cm^{-1}, which is assigned to the symmetric bending of the CH_3 groups in thiram. Note that this Raman band is strongly enhanced in relation to the band observed at 561 cm^{-1}, assigned to the disulfide vibrational modes, which is clearly observed by comparing the conventional Raman spectrum of solid thiram with the corresponding SERS spectra (Figure 4). We suggest that this is a consequence not only of the enhancement of the Raman band at 1374 cm^{-1}, but also of partial reduction of thiram molecules chemisorbed at the metal surface via cleavage of S-S bonds. This hypothesis is further supported by the absence of the band at 390 cm^{-1} in the SERS spectra, which is assigned to the S-S stretching vibration in the Raman spectrum of thiram. Moreover, the appearance of the SERS band located at 1502 cm^{-1}, indicates the predominance of the thioureide tautomer as the main adsorbate on the metal surface. The enhancement of the band at 1374 cm^{-1} on the SERS spectra is attributed to the shortening of the CH_3 and CN groups distance to the metal surface[43].

Figure 4 also shows that the observed Raman enhancement decreases as the content of Ag in the metal colloids also decreases. This is in line with previous reports where the less noble metal can more easily promote the cleavage of the S-S bond, resulting in higher SERS sensitivity towards this type of analytes with disulfide bond[51]. Overall, the SERS spectra indicate that the presence of Ag in the nanoalloys is important to observe strong enhancement. Interestingly, while for the SERS experiments involving the colloids, the minimum SERS detection limit achieved was $1x10^{-6}$ M[43], herein, it was possible to further improve the SERS sensitivity towards thiram, where a SERS minimum detection limit of $1x10^{-7}$ M was obtained. This improved SERS sensitivity might be related to a change in conformation of the PAMAM dendrimer on the surface of the assemblies after inkjet deposition, as will be discussed below. We have made SERS measurements in similar conditions, using different molar ratios in the nanoalloys, but despite the similar SERS performance for the substrates printed with 5:15 and 10:10 Au:Ag:PAMAM, the former exhibited best SERS activity at lower thiram concentration, reaching $1x10^{-7}$ M as the lower limit of SERS detection (Figure 5). Therefore the 5:15 Au:Ag:PAMAM colloid was selected for the subsequent studies as described below.

Figure 5 shows the SERS spectra and Raman images of thiram, deposited from aqueous samples of different concentrations, on substrates after 20 printing cycles of the 5:15 Au:Ag:PAMAM colloids on paper. Raman spectroscopy coupled with imaging methods provides important spectral and spatial information and thus allows for the localized identification of thiram species in the substrate. The brighter areas in the Raman maps indicate a strong signal arising from

thiram adsorbed to the metal in those regions. Consequently, the Raman maps also confirm that the metal nanoassemblies are distributed across the paper substrate. In addition, the effect of the number of printing cycles is detailed in Figure S6 (supporting information). As expected, the SERS activity towards thiram increases as the number of printing cycles increases due to the higher number of particles imprinted on the cellulose fibres. However, there is an optimum number of printing cycles, after which a further decrease or increase in the number of particles resulted in detrimental SERS performance. While the deposition of only 10 printing cycles resulted in the absence of SERS activity for all the substrates; an increase in the number of deposited particles beyond the optimal conditions also resulted in detrimental SERS signal due to extensive aggregation and consequent delocalization of the electric field of the resulting larger clusters (Figure S7-S8, supporting information)[34].

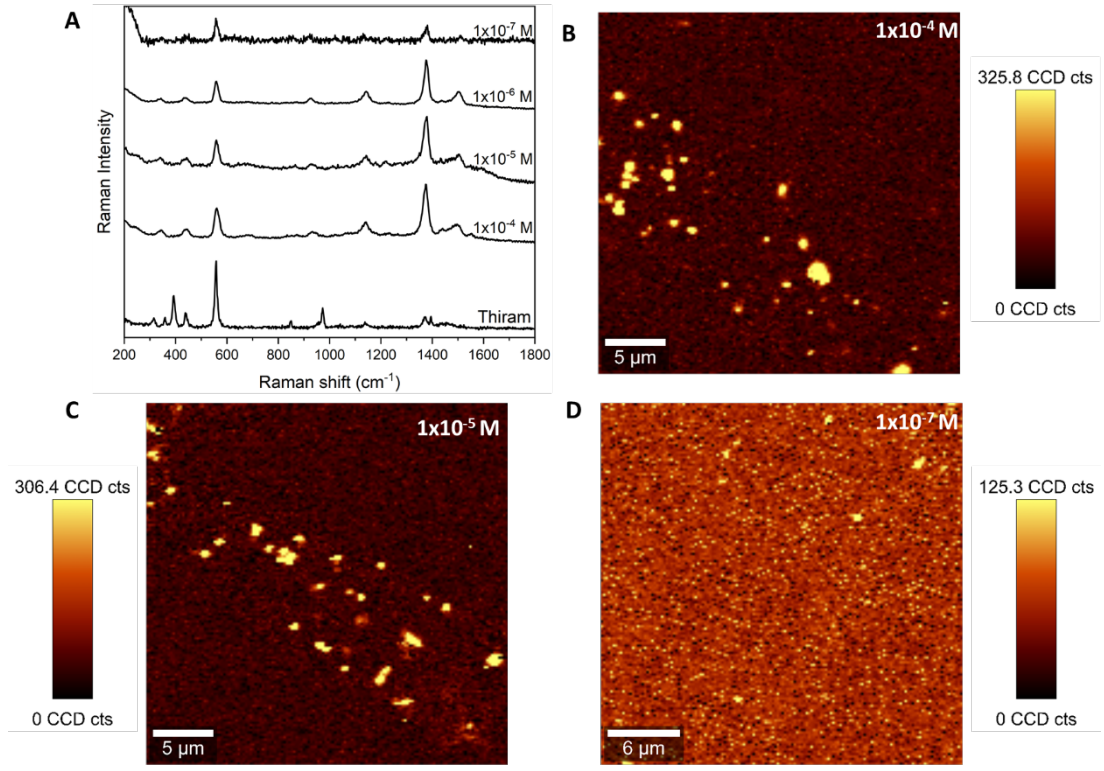

Figure 5 –SERS spectra of thiram at the indicated concentrations using the 5:15 Au:Ag:PAMAM substrate after 20 printing cycles (A) and the corresponding Raman images by monitoring the band at 1374 cm^{-1} (B-D).

3.2.2. Hydrophobic paper substrates containing 5:15 Au:Ag PAMAM-stabilized nanoassemblies

SERS performance of a paper substrate prepared by inkjet printing methods can be improved by modifying its surface properties prior the deposition of the plasmonic nanoparticles[52]. In

particular, the wettability properties of the paper are very important, as demonstrated by several authors showing better SERS performance for hydrophobic substrates[33, 53]. We have ourselves demonstrated good SERS performance for hydrophobic paper substrates obtained by a one-step fabrication, using ink formulations containing PS aqueous emulsions[34]. Unlike this previous work, here the use of PAMAM dendrimers in the PS emulsion resulted in immediate particle agglomeration, thus precluding the application of such method due to clogging of the ejection nozzle. Instead, paper sheets have been submitted to 15 printing cycles of a PS emulsion before printing the colloid 5:15 Au:Ag:PAMAM, which was selected due to the highest SERS sensitivity, likely due to the higher molar content of Ag. The deposition of PS was then monitored by SEM using the secondary electron (SE) and the back-scattered electron (BSE) modes. Both modes provide important information regarding the surface nature of the resulting paper substrate. On one hand, the SE mode deliver images with good topographic contrast, while on the other hand, the BSE results on imagens where the contrast depends on the atomic weight. Consequently, in Figure 6-A it is possible to observe the extensive and uniform distribution of the PS spheres along the cellulose fibres. The analysis of the SEM micrographs after deposition of the 5:15 Au:Ag:PAMAM nanoassemblies on the hydrophobic paper is not a trivial task, given the chemical components on the resulting substrates. Nevertheless, in certain regions of the paper, it was possible to observe the presence of structures that were ascribed to the metal alloyed nanoassemblies (Figure 6-D). The presence of these structures was also inferred by optical measurements, which show great similarities between both ink-jet printed substrates, i.e. PS treated and non-treated papers printed with 5:15 Au:Ag:PAMAM nanoassemblies (Figure 6-E). As expected, the water contact angle (WCA) measurements of the paper treated with PS revealed an increase in hydrophobicity when compared with the bare office paper, exhibiting WCA values that changed from 78.4° ± 2.9 to 148.2° ± 1.5 (Figure 6-F). Paper substrates submitted to further 10 to 20 printing cycles have shown a slight decrease of the WCA values, which can be explained by the presence of an higher amount of the PAMAM dendrimer and the hydrophilic nature of its amine terminal groups[54]. This is not enough to disrupt the hydrophobic nature of the office paper treated with PS, because even so the amine terminal groups are less exposed as compared to the globular shape adopted in solution, given the oblate conformation of the PAMAM dendrimer molecules on the solid substrate [55, 56].

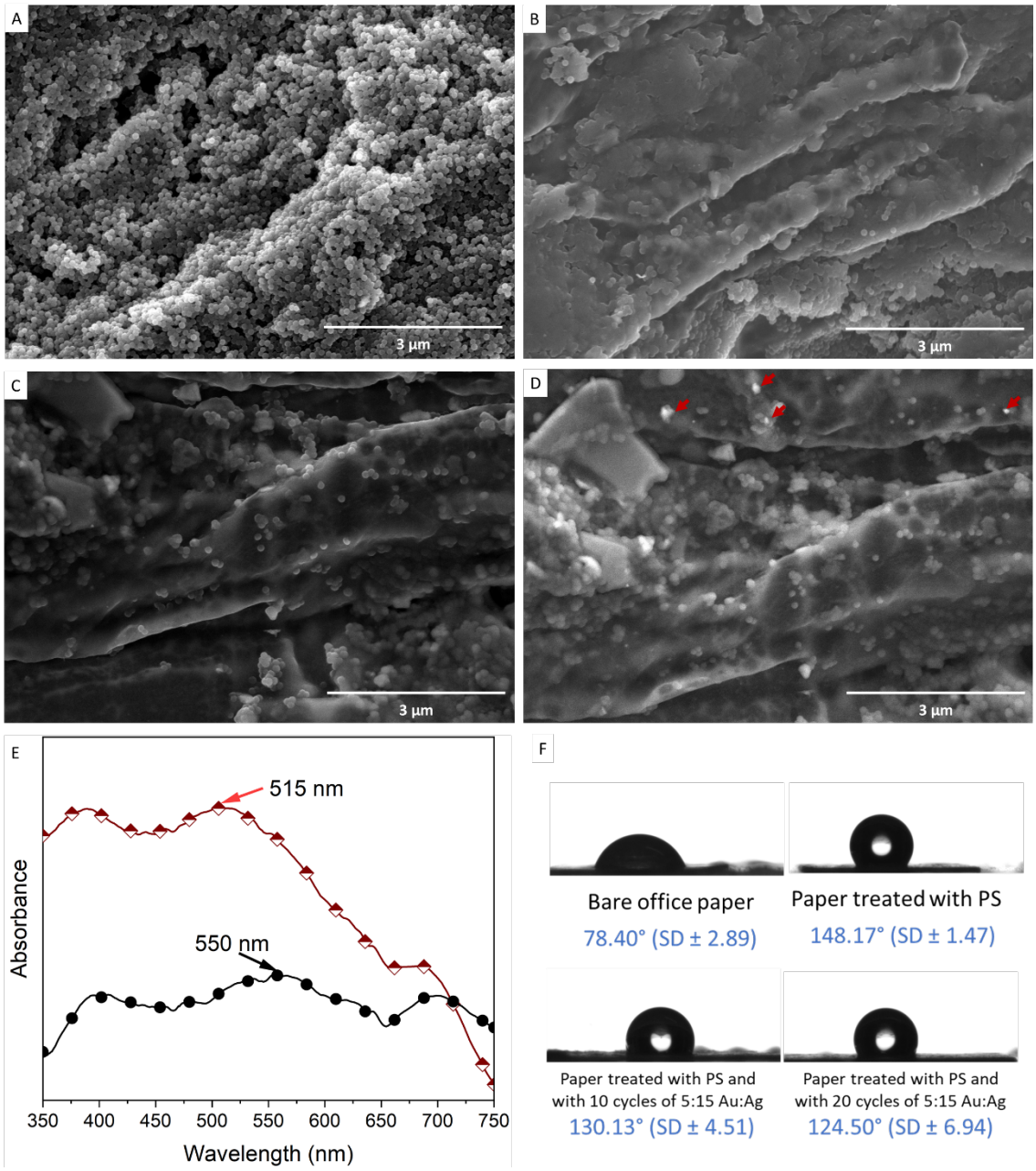

Figure 6 – SEM micrographs of paper treated with PS on SE mode (A) and BSE mode (B) and of the same paper after deposition with 5:15 Au:Ag:PAMAM dendrimer-stabilized nanoassemblies (red arrows mark the presence of nanoassemblies) ((C) SE mode and (D) BSE mode); the optical spectra of the paper substrates containing the 5:15 Au:Ag nanoassemblies on office paper (—●—) and on hydrophobic paper (—◆—) (E) and the WCA measurements of bare paper, PS treated paper and of the PS treated paper with 10-20 printing cycles of the 5:15 Au:Ag:PAMAM nanoparticles (F).

Figure 7 details the performance of the hydrophobic paper substrates after inkjet printing of 5:15 Au:Ag:PAMAM colloids, in the SERS detection of thiram. Firstly, the hydrophobic character of the paper substrates resulted in better signal enhancement for a lower number of printing cycles of the metal colloids (Figure 7-A); for instance, no Raman signal of thiram was observed for 10 printing cycles on paper without PS treatment, but a minimum detection of $1x10^{-6}$ M was achieved in similar conditions using paper sheets previously submitted to inkjet printing of the PS emulsion. Similar behaviour was observed for paper substrates after 15 printing cycles of the 5:15 Au:Ag:PAMAM colloids, whereas the SERS sensitivity improved from $1x10^{-5}$ M to $1x10^{-6}$ M (Figure 7-A). Although the limit of SERS detection did not decrease for the substrates submitted to 20 printing cycles of 5:15 Au:Ag:PAMAM, in relation to the corresponding paper not treated with PS, there was a significant improvement regarding the signal-to-noise ratio (SNR) (Figure S9 and Table S2, supporting information).

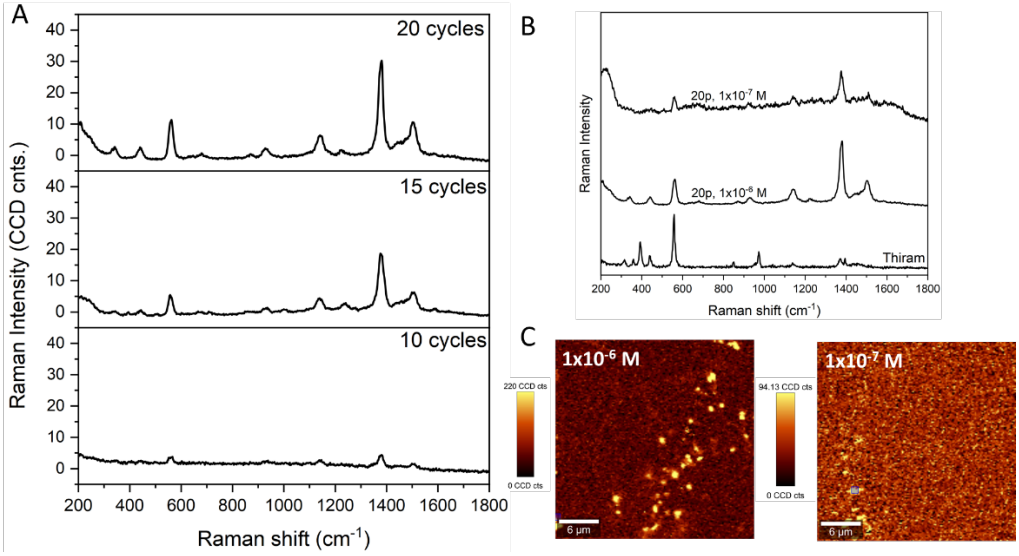

Figure 7 – SERS activity of 5:15 Au:Ag:PAMAM nanoassemblies in the detection of thiram on paper pre-treated with PS and containing 10 to 20 printing cycles of nanoassemblies ($1x10^{-6}$ M of thiram) (A). SERS spectra of thiram using paper substrates pre-treated with PS and 20 printing cycles of 5:15 Au:Ag:PAMAM nanoassemblies (B) and the corresponding Raman images (C).

3.2.3. Topographic analysis of the hydrophobic paper substrates

The better SERS sensitivity observed when using hydrophobic paper substrates has been related to the occurrence of less spreading of water droplets containing the target molecules under analysis, which results in a concentration effect in a smaller area of the substrate[33, 57-59]. Indeed, in this research the paper substrates revealed a better SERS performance towards thiram when compared with the corresponding metal colloids reported previously [43]. We

suggest that together with this hydrophobic effect in our substrates, the increase in SERS performance is also due to the change in the dendrimer architecture after deposition on the paper, changing from a globular structure in solution to an oblate configuration on the underlying surface modified fibres[55, 56, 60, 61]. This "collapse" of the dendrimer architecture results in the increase of the metal surface exposed for chemisorption of the analyte molecules, thus leading to improved SERS sensitivity. Indeed, several works have explored the deposition of PAMAM dendrimers on different kinds of surfaces and their effect on the structure of the dendrimer[60-66]. For example, it is known that depending on the concentration, PAMAM dendrimers having amine terminal groups can easily spread on mica surfaces resulting in the formation of uniform films[61]. Figures 8 and S10 show the topographic analysis of the paper substrates by AFM that corroborates the hypothesis put forward above.

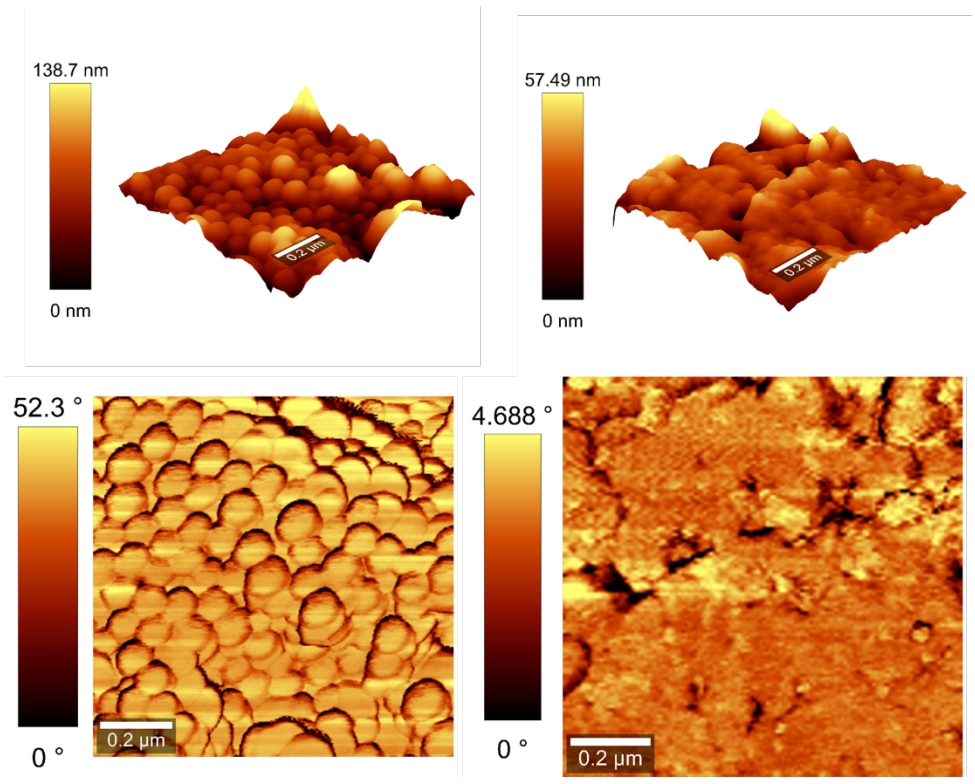

Figure 8 – 3D topography (top) and phase (bottom) AFM images (1μm x 1μm) of paper treated with PS (left) and paper pre-treated with PS and submitted to 20 printing cycles of 5:15 Au:Ag:PAMAM nanoassemblies (right).

As detailed in Figure 8 (left panel), the inkjet printing of PS emulsion on office paper resulted in the uniform distribution of the polymer beads over the surface of the fibres, as also observed by SEM (Figure 6). In addition, the topography profile agrees with the typical size of the

individual spheres of about 100 nm (Figure S10). However, the inkjet deposition of the 5:15 Au:Ag:PAMAM nanoassemblies on the PS coated paper resulted in a marked change of the surface topography (Figure 8, right panel). In this case, the well-defined discrete PS spheres are no longer observed over the cellulose fibres, which instead show a smoother coating, which is also in agreement with the SEM images (Figures 6-A and 6-C). As expected, the surface roughness of the paper substrates varied depending on the inkjet printing material, while paper containing only the PS coat exhibited a root mean square (Rms) of 33.95 ± 7.26 nm, the corresponding paper substrate with 5:15 Au:Ag:PAMAM nanoassemblies displayed a Rms of 18.75 ± 0.54 nm (Table S3). The same behaviour was also observed for the paper, where no PS treatment was done. Accordingly, after the deposition of the 5:15 Au:Ag:PAMAM alloy nanoassemblies on standard paper without PS, a decrease in the surface roughness is also observed when compared with the bare paper (Table S3). In this latter substrate, the topography profile also reveals the presence of structures that are similar in size and shape to the alloy nanoassemblies observed in TEM and SEM (Figure S10-C). This trend observed on the surface of the paper after inkjet deposition of the colloids can be attributed to the collapse of the dendrimer structure, resulting in compressed, oblate spheroids. Figure 8 also shows AFM images on phase mode that confirm such distinct surface characteristics for paper coated only with PS in comparison to paper pre-treated with PS and ink jet printed with Au:Ag:PAMAM nanoassemblies. As noted before, PAMAM dendrimers are soft macromolecules with a fairly open structure and consequently, when deposited on solid surfaces, they tend to deform due to the interaction between the dendrimer functional groups and the surface of the substrate[61]. However, in the case of paper substrates pre-treated with PS, during the inkjet printing process an interface region is formed, in which the electrostatic interactions are favoured between the positively charged PAMAM dendrimers and the negatively charged PS spheres due to the presence of SDS as surfactant. This process resulted in topographical changes on the coated cellulosic fibres, as demonstrated by the AFM and SEM images. The AFM analysis of the above paper substrates after deposition of thiram (Figure S10-B and -D) retain the topographic profile, further reinforcing the hypothesis that the conformational change of the dendrimer structure after deposition may contribute to improved SERS sensitivity. Furthermore, the deposition of the PAMAM stabilized nanoassemblies may change the surface charge density of the paper substrates previously treated with PS, due to conformational changes on the dendrimer structure after deposition [67-70].

Finally, the repeatability and long-term SERS signal stability were assessed for the best performing paper substrates, i.e. those pre-treated with PS and printed with 20 printing cycles

of 5:15 Au:Ag:PAMAM nanoassemblies. Figure 9-A shows the SERS signal variability of three substrates, where for each substrate 30 data points were collected from the Raman images. The relative standard deviation (RSD) of three independent analyses revealed to be 11.37% while the RSD within each substrate ranged from 13.76% to 36.02%. The variation observed within each substrate is within acceptable ranges for this class of materials given the structural heterogeneity of the paper surface. Despite that, the RSD of three independent substrates was 11.37%, thus confirming the repeatability for the reported substrates which are similar to previously reported hydrophobic substrates for SERS applications[57, 59]. The stability of the PS treated paper substrates with the 5:15 Au:Ag:PAMAM nanoassemblies was investigated by Raman imaging and using thiram ($1x10^{-5}$ M) as the analyte. Figure 8-B shows that no significant changes were observed in the SERS spectra of thiram after 90 days, suggesting good stability of the substrates over time.

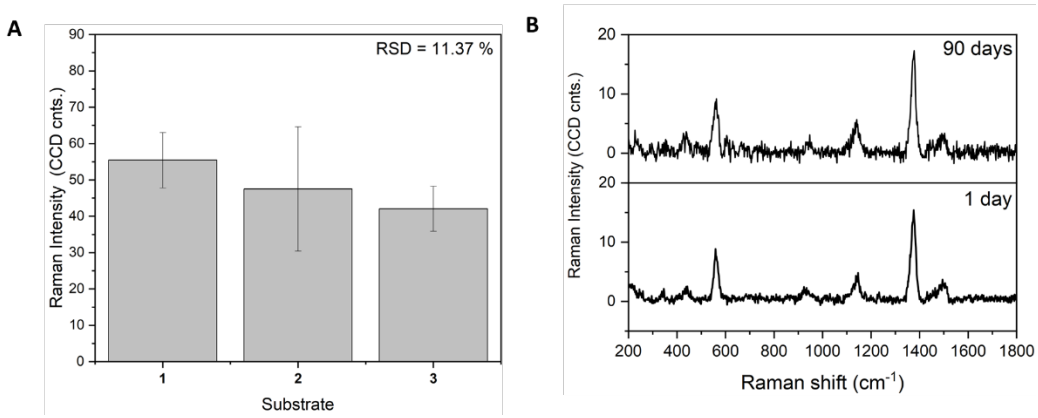

Figure 9 – Variation of the thiram SERS band intensity at 1374 cm^{-1} for the paper treated with PS and with 5:15 Au:Ag:PAMAM alloy nanoassemblies (A). Each bar corresponds to an independent analysis that represents the average intensity calculated from 30 data points of the Raman images; the SERS spectra of thiram ($1x10^{-5}$ M) observed for the same substrate after 1 day and 90 days (B).

4. Conclusions

We reported here for the first time the inkjet printing of dendrimer-stabilized Au:Ag nanoalloys on office paper, aiming at the fabrication of handy and efficient SERS substrates. In particular, we have demonstrated the crucial role of the PAMAM dendrimer in the ink formulations for this application. Firstly, it acts as a “glue-like” molecular structure for the clustering of Au and Ag nanoparticles in the colloidal alloys. In addition, it was used as the sole reducing and stabilizing agent for the preparation of the Au:Ag alloys, providing a straightforward approach to obtain

nanostructures with variable plasmonic behaviour. The dendrimer-stabilized Au:Ag nanoassemblies that resulted from this research were successfully deposited on office paper through inkjet printing. The ensuing substrates displayed good SERS sensitivity for the detection of model pesticide thiram dissolved in aqueous solutions. In particular, the Au:Ag:PAMAM nanoassemblies have shown the highest SERS activity when deposited on hydrophobic paper substrates, i.e. pre-treated with a polystyrene aqueous emulsion. A plausible explanation for this behaviour relies on the occurrence of an interface region during the printing step, in which electrostatic interactions between both polymers (PS and PAMAM) became favoured and alter the surface coating of the fibres. As consequence, the globular structure of the dendrimer molecules is deformed leading to more metal surfaces exposed for chemisorption. An interesting follow up of this topic, is the use of AFM colloidal probe measurements to understand the effect of PAMAM deposition on surface charge density and its possible interaction with the surfactant SDS of the PS spheres.[67-70]

Finally, it should be noted that the resulting paper substrates are characterized by its "biofriendliness" and relatively low-cost. In fact, the printing method used in this work, allows the preparation of hundreds of spots in a single paper sheet, where the total amount of PAMAM dendrimer and polystyrene deposited on the paper substrates represents a small fraction of the total components (<0.5% w/v). In brief, this research opens an avenue for preparing dendrimer-based metal colloids for inkjet printing on a variety of chemically modified surfaces, making more flexible the design and fabrication of SERS probing platforms.

CRediT authorship contribution statement

Tiago Fernandes: Conceptualization, Methodology, Validation, Formal Analysis, Investigation, Writing- Original Draft, Writing- Review & Editing. **Natércia Martins**: Methodology, Validation, Investigation, Writing- Review & Editing. **Sara Fateixa**: Methodology, Validation, Writing- Review & Editing. **Helena Nogueira**: Formal analysis, Resources, Writing- Review & Editing. **Ana Daniel-da-Silva**: Formal Analysis, Writing- Review & Editing, Supervision, Funding acquisition. **Tito Trindade**: Conceptualization, Methodology, Formal Analysis, Resources, Writing- Review & Editing, Supervision, Funding acquisition.

Declaration of Competing Interest

The authors declare that they have no known competing interests or personal relationships that could have appeared to influence the work reported in this paper.

Acknowledgements

T.F. thanks the Fundação para a Ciência e Tecnologia (FCT) for the PhD grant SFRH/BD/130934/2017. N.C.T.M. and S.F. are funded by national funds (OE), through FCT-Fundação para a Ciência e Tecnologia,I.P., in the scope of the framework contract foreseen in the numbers 4, 5, and 6 of the article 23, of the Decree-Law 57/2016, of August 29, changed by the law 57/2017, of July 19. A. L. D. Silva acknowledges FCT for the research contract under the Program 'Investigador FCT' 2014. This work was developed within the scope of the project CICECO-Aveiro Institute of Materials, FCT Ref. UIDB/50011/2020 & UIDP/50011/2020.

References

[1] L. Nayak, S. Mohanty, S.K. Nayak, A. Ramadoss, A review on inkjet printing of nanoparticle inks for flexible electronics, Journal of Materials Chemistry C 7(29) (2019) 8771-8795.
[2] C. Cano-Raya, Z.Z. Denchev, S.F. Cruz, J.C. Viana, Chemistry of solid metal-based inks and pastes for printed electronics – A review, Applied Materials Today 15 (2019) 416-430.
[3] H. Kang, G.H. Lee, H. Jung, J.W. Lee, Y. Nam, Inkjet-Printed Biofunctional Thermo-Plasmonic Interfaces for Patterned Neuromodulation, ACS Nano 12(2) (2018) 1128-1138.
[4] H. Kang, J.W. Lee, Y. Nam, Inkjet-Printed Multiwavelength Thermoplasmonic Images for Anticounterfeiting Applications, ACS Appl Mater Interfaces 10(7) (2018) 6764-6771.
[5] S. Sardar, P. Wojcik, E.S.H. Kang, R. Shanker, M.P. Jonsson, Structural coloration by inkjet-printing of optical microcavities and metasurfaces, Journal of Materials Chemistry C 7(28) (2019) 8698-8704.
[6] N. Karim, S. Afroj, S. Tan, K.S. Novoselov, S.G. Yeates, All Inkjet-Printed Graphene-Silver Composite Ink on Textiles for Highly Conductive Wearable Electronics Applications, Sci Rep 9(1) (2019) 8035.
[7] H. Shahariar, I. Kim, H. Soewardiman, J.S. Jur, Inkjet Printing of Reactive Silver Ink on Textiles, ACS Appl Mater Interfaces 11(6) (2019) 6208-6216.
[8] S. Majee, M.C.F. Karlsson, A. Sawatdee, M.Y. Mulla, N.u.H. Alvi, V. Beni, D. Nilsson, Low temperature chemical sintering of inkjet-printed Zn nanoparticles for highly conductive flexible electronic components, npj Flexible Electronics 5(1) (2021) 14.
[9] H. Maleki, V. Bertola, Recent advances and prospects of inkjet printing in heterogeneous catalysis, Catalysis Science & Technology 10(10) (2020) 3140-3159.
[10] W.H. Chou, A. Gamboa, J.O. Morales, Inkjet printing of small molecules, biologics, and nanoparticles, Int J Pharm 600 (2021) 120462.
[11] P.A.A.P. Marques, H.I.S. Nogueira, R.J.B. Pinto, C.P. Neto, T. Trindade, Silver-bacterial cellulosic sponges as active SERS substrates, Journal of Raman Spectroscopy 39(4) (2008) 439-443.
[12] S. Fateixa, M. Wilhelm, A.M. Jorge, H.I.S. Nogueira, T. Trindade, Raman imaging studies on the adsorption of methylene blue species onto silver modified linen fibers, Journal of Raman Spectroscopy 48(6) (2017) 795-802.
[13] D. Bugakova, V. Slabov, E. Sergeeva, M. Zhukov, A.V. Vinogradov, Comprehensive characterization of TiO2 inks and their application for inkjet printing of microstructures, Colloids and Surfaces A: Physicochemical and Engineering Aspects 586 (2020) 124146.
[14] M. Kuang, L. Wu, Z. Huang, J. Wang, X. Zhang, Y. Song, Inkjet Printing of a Micro/Nanopatterned Surface to Serve as Microreactor Arrays, ACS Appl Mater Interfaces 12(27) (2020) 30962-30971.

564 [15] C.M. González-Henríquez, F.E. Rodriguez-Umanzor, M.A. Sarabia-Vallejos, C.A. Terraza, E.
565 Martínez-Campos, J. Rodriguez-Hernandez, Innovative procedure for precise deposition of
566 wrinkled hydrogel films using direct inkjet printing, Materials & Design 194 (2020) 108959.
567 [16] R. Pagano, M. Ottolini, L. Valli, S. Bettini, G. Giancane, Ag nanodisks decorated filter paper
568 as a SERS platform for nanomolar tetracycline detection, Colloids and Surfaces A:
569 Physicochemical and Engineering Aspects 624 (2021) 126787.
570 [17] Y. Xu, X. Gao, C. Yang, B. Man, J. Leng, Fork-shaped paper SERS sensors coated with
571 raspberry-like bimetallic nanospheres for the detection of the boosted mixture: experimental
572 design and applications, Journal of Materials Chemistry C 9(8) (2021) 2763-2774.
573 [18] M. Liu, A. Bhandari, M.A. Haqqani Mohammed, D.R. Radu, C.-Y. Lai, Versatile Silver
574 Nanoparticles-Based SERS Substrate with High Sensitivity and Stability, Applied Nano 2(3) (2021)
575 242-256.
576 [19] M.L. Xu, Y. Gao, X.X. Han, B. Zhao, Detection of Pesticide Residues in Food Using Surface-
577 Enhanced Raman Spectroscopy: A Review, J Agric Food Chem 65(32) (2017) 6719-6726.
578 [20] J. Perumal, Y. Wang, A.B.E. Attia, U.S. Dinish, M. Olivo, Towards a point-of-care SERS sensor
579 for biomedical and agri-food analysis applications: a review of recent advancements, Nanoscale
580 13(2) (2021) 553-580.
581 [21] M. Girmatsion, A. Mahmud, B. Abraha, Y. Xie, Y. Cheng, H. Yu, W. Yao, Y. Guo, H. Qian, Rapid
582 detection of antibiotic residues in animal products using surface-enhanced Raman Spectroscopy:
583 A review, Food Control 126 (2021) 108019.
584 [22] B. Hu, D.W. Sun, H. Pu, Q. Wei, Rapid nondestructive detection of mixed pesticides residues
585 on fruit surface using SERS combined with self-modeling mixture analysis method, Talanta 217
586 (2020) 120998.
587 [23] J. Chen, M. Huang, L. Kong, M. Lin, Jellylike flexible nanocellulose SERS substrate for rapid
588 in-situ non-invasive pesticide detection in fruits/vegetables, Carbohydr Polym 205 (2019) 596-
589 600.
590 [24] K. Wang, D.W. Sun, H. Pu, Q. Wei, Polymer multilayers enabled stable and flexible Au@Ag
591 nanoparticle array for nondestructive SERS detection of pesticide residues, Talanta 223(Pt 2)
592 (2021) 121782.
593 [25] R. Pilot, R. Signorini, C. Durante, L. Orian, M. Bhamidipati, L. Fabris, A Review on Surface-
594 Enhanced Raman Scattering, Biosensors (Basel) 9(2) (2019) 57.
595 [26] R. Pilot, SERS detection of food contaminants by means of portable Raman instruments,
596 Journal of Raman Spectroscopy 49(6) (2018) 954-981.
597 [27] J. Sun, L. Gong, W. Wang, Z. Gong, D. Wang, M. Fan, Surface-enhanced Raman spectroscopy
598 for on-site analysis: A review of recent developments, Luminescence 35(6) (2020) 808-820.
599 [28] J.-S. Wi, J.D. Kim, W. Lee, H. Choi, M. Kwak, J. Song, T.G. Lee, J.G. Ok, Inkjet−Printable
600 Nanoporous Ag Disk Arrays Enabling Coffee−Ring Effect−Driven Analyte Enrichment Towards
601 Practical SERS Applications, International Journal of Precision Engineering and Manufacturing-
602 Green Technology (2021).
603 [29] S.M. Restaino, I.M. White, A critical review of flexible and porous SERS sensors for analytical
604 chemistry at the point-of-sample, Anal Chim Acta 1060 (2019) 17-29.
605 [30] P. Joshi, V. Santhanam, Inkjet-Based Fabrication Process with Control over the Morphology
606 of SERS-Active Silver Nanostructures, Industrial & Engineering Chemistry Research 57(15) (2018)
607 5250-5258.
608 [31] X. Kong, Y. Xi, P. Le Duff, X. Chong, E. Li, F. Ren, G.L. Rorrer, A.X. Wang, Detecting explosive
609 molecules from nanoliter solution: A new paradigm of SERS sensing on hydrophilic photonic
610 crystal biosilica, Biosens Bioelectron 88 (2017) 63-70.
611 [32] J.M. Romo-Herrera, K. Juarez-Moreno, L. Guerrini, Y. Kang, N. Feliu, W.J. Parak, R.A. Alvarez-
612 Puebla, Paper-based plasmonic substrates as surface-enhanced Raman scattering spectroscopy
613 platforms for cell culture applications, Mater Today Bio 11 (2021) 100125.

[33] L. Xian, R. You, D. Lu, C. Wu, S. Feng, Y. Lu, Surface-modified paper-based SERS substrates for direct-droplet quantitative determination of trace substances, Cellulose 27(3) (2019) 1483-1495.
[34] N.C.T. Martins, S. Fateixa, T. Fernandes, H.I.S. Nogueira, T. Trindade, Inkjet Printing of Ag and Polystyrene Nanoparticle Emulsions for the One-Step Fabrication of Hydrophobic Paper-Based Surface-Enhanced Raman Scattering Substrates, ACS Applied Nano Materials 4(5) (2021) 4484-4495.
[35] M. Dustov, D.I. Golovina, A.Y. Polyakov, A.E. Goldt, A.A. Eliseev, E.A. Kolesnikov, I.V. Sukhorukova, D.V. Shtansky, W. Grunert, A.V. Grigorieva, Silver Eco-Solvent Ink for Reactive Printing of Polychromatic SERS and SPR Substrates, Sensors (Basel) 18(2) (2018) 521.
[36] G. Weng, Y. Yang, J. Zhao, J. Li, J. Zhu, J. Zhao, Improving the SERS enhancement and reproducibility of inkjet-printed Au NP paper substrates by second growth of Ag nanoparticles, Materials Chemistry and Physics 253 (2020) 123416.
[37] Y. Li, O. Dahhan, C.D.M. Filipe, J.D. Brennan, R.H. Pelton, Deposited Nanoparticles Can Promote Air Clogging of Piezoelectric Inkjet Printhead Nozzles, Langmuir 35(16) (2019) 5517-5524.
[38] F. Avila-Salas, R.I. Gonzalez, P.L. Rios, I. Araya-Duran, M.B. Camarada, Effect of the Generation of PAMAM Dendrimers on the Stabilization of Gold Nanoparticles, J Chem Inf Model 60(6) (2020) 2966-2976.
[39] R.J. Smith, C. Gorman, S. Menegatti, Synthesis, structure, and function of internally functionalized dendrimers, Journal of Polymer Science 59(1) (2020) 10-28.
[40] B. Devadas, A.P. Periasamy, K. Bouzek, A review on poly(amidoamine) dendrimer encapsulated nanoparticles synthesis and usage in energy conversion and storage applications, Coordination Chemistry Reviews 444 (2021) 214062.
[41] C. Song, M. Shen, J. Rodrigues, S. Mignani, J.-P. Majoral, X. Shi, Superstructured poly(amidoamine) dendrimer-based nanoconstructs as platforms for cancer nanomedicine: A concise review, Coordination Chemistry Reviews 421 (2020) 213463.
[42] F.M. Winnik, A.R. Davidson, M.P. Breton, Inks with Dendrimer Colorants, Xerox Corporation, 1992.
[43] T. Fernandes, S. Fateixa, M. Ferro, H.I.S. Nogueira, A.L. Daniel-da-Silva, T. Trindade, Colloidal dendritic nanostructures of gold and silver for SERS analysis of water pollutants, Journal of Molecular Liquids 337 (2021) 116608.
[44] A.S. Pereira, P. Rauwel, M.S. Reis, N.J. Oliveira Silva, A. Barros-Timmons, T. Trindade, Polymer encapsulation effects on the magnetism of EuS nanocrystals, Journal of Materials Chemistry 18(38) (2008) 4572-4578.
[45] T. Liu, D.R. Baek, J.S. Kim, S.W. Joo, J.K. Lim, Green Synthesis of Silver Nanoparticles with Size Distribution Depending on Reducing Species in Glycerol at Ambient pH and Temperatures, ACS Omega 5(26) (2020) 16246-16254.
[46] R.L. McCreery, Signal-to-Noise in Raman Spectroscopy, in: J.D. Winefordner (Ed.), Raman Spectroscopy for Chemical Analysis2005, pp. 49-71.
[47] R. Pöykiö, H. Nurmesniemi, Calcium carbonate waste from an integrated pulp and paper mill as a potential liming agent, Environmental Chemistry Letters 6(1) (2007) 47-51.
[48] S. Sánchez-Cortés, M. Vasina, O. Francioso, J.V. García-Ramos, Raman and surface-enhanced Raman spectroscopy of dithiocarbamate fungicides, Vibrational Spectroscopy 17 (1998) 133-144.
[49] S. Sánchez-Cortés, C. Domingo, J.V. García-Ramos, J.A. Aznárez, Surface-Enhanced Vibrational Study (SEIR and SERS) of Dithiocarbamate Pesticides on Gold Films, Langmuir 17 (2001) 1157-1162.
[50] S. Fateixa, M. Raposo, H.I.S. Nogueira, T. Trindade, A general strategy to prepare SERS active filter membranes for extraction and detection of pesticides in water, Talanta, 2018, pp. 558-566.

[51] E. López-Tobar, B. Hernández, M. Ghomi, S. Sanchez-Cortes, Stability of the Disulfide Bond in Cystine Adsorbed on Silver and Gold Nanoparticles As Evidenced by SERS Data, The Journal of Physical Chemistry C 117(3) (2013) 1531-1537.
[52] S.A. Ogundare, W.E. van Zyl, A review of cellulose-based substrates for SERS: fundamentals, design principles, applications, Cellulose 26(11) (2019) 6489-6528.
[53] H. Sun, X. Li, Z. Hu, C. Gu, D. Chen, J. Wang, B. Li, T. Jiang, X. Zhou, Hydrophilic-hydrophobic silver nanowire-paper based SERS substrate for in-situ detection of furazolidone under various environments, Applied Surface Science 556 (2021) 149748.
[54] H. Tokuhisa, M. Zhao, L.A. Baker, V.T. Phan, D.L. Dermody, M.E. Garcia, R.F. Peez, R.M. Crooks, T.M. Mayer, Preparation and Characterization of Dendrimer Monolayers and Dendrimer−Alkanethiol Mixed Monolayers Adsorbed to Gold, Journal of the American Chemical Society 120(18) (1998) 4492-4501.
[55] D.C. Tully, J.M.J. Fréchet, Dendrimers at surfaces and interfaces: chemistry and applications, Chemical Communications (14) (2001) 1229-1239.
[56] F.T. Xu, S.C. Street, J.A. Barnard, Pattern Formation in Aerosol-Deposited Dendrimer Films, Langmuir 19(7) (2003) 3066-3070.
[57] N.V. Godoy, D. García-Lojo, F.A. Sigoli, J. Pérez-Juste, I. Pastoriza-Santos, I.O. Mazali, Ultrasensitive inkjet-printed based SERS sensor combining a high-performance gold nanosphere ink and hydrophobic paper, Sensors and Actuators B: Chemical 320 (2020) 128412.
[58] J. Duan, Z. Qiu, L. Li, L. Feng, L. Huang, G. Xiao, Inkjet printed silver nanoparticles on hydrophobic papers for efficient detection of thiram, Spectrochim Acta A Mol Biomol Spectrosc 243 (2020) 118811.
[59] T.N.Q. Trang, L.Q. Vinh, T.T. Doanh, V.T.H. Thu, Structure-adjustable colloidal silver nanoparticles on polymers grafted cellulose paper-based highly sensitive and selective SERS sensing platform with analyte enrichment function, Journal of Alloys and Compounds 867 (2021) 159158.
[60] T. Müller, D.G. Yablon, R. Karchner, D. Knapp, M.H. Kleinman, H. Fang, C.J. Durning, D.A. Tomalia, N.J. Turro, G.W. Flynn, AFM Studies of High-Generation PAMAM Dendrimers at the Liquid/Solid Interface, Langmuir 18(20) (2002) 7452-7455.
[61] J. Li, L.T. Piehler, D. Qin, J.R. Baker, D.A. Tomalia, D.J. Meier, Visualization and Characterization of Poly(amidoamine) Dendrimers by Atomic Force Microscopy, Langmuir 16(13) (2000) 5613-5616.
[62] V.N. Bliznyuk, F. Rinderspacher, V.V. Tsukruk, On the structure of polyamidoamine dendrimer monolayers, Polymer 39(21) (1998) 5249-5252.
[63] A. Hierlemann, J.K. Campbell, L.A. Baker, R.M. Crooks, A.J. Ricco, Structural Distortion of Dendrimers on Gold Surfaces: A Tapping-Mode AFM Investigation, Journal of the American Chemical Society 120(21) (1998) 5323-5324.
[64] J. Li, D. Qin, J.R. Baker Jr, D.A. Tomalia, The characterization of high generation poly(amidoamine) G9 dendrimers by atomic force microscopy (AFM), Macromolecular Symposia 167(1) (2001) 257-269.
[65] T.A. Betley, M.M. Banaszak Holl, B.G. Orr, D.R. Swanson, D.A. Tomalia, J.R. Baker, Tapping Mode Atomic Force Microscopy Investigation of Poly(amidoamine) Dendrimers: Effects of Substrate and pH on Dendrimer Deformation, Langmuir 17(9) (2001) 2768-2773.
[66] T.A. Betley, J.A. Hessler, A. Mecke, M.M. Banaszak Holl, B.G. Orr, S. Uppuluri, D.A. Tomalia, J.R. Baker, Tapping Mode Atomic Force Microscopy Investigation of Poly(amidoamine) Core−Shell Tecto(dendrimers) Using Carbon Nanoprobes, Langmuir 18(8) (2002) 3127-3133.
[67] R. Pericet-Camara, B.P. Cahill, G. Papastavrou, M. Borkovec, Nano-patterning of solid substrates by adsorbed dendrimers, Chemical Communications (3) (2007) 266-268.
[68] P.M. Welch, C.F. Welch, N.J. Henson, Flattening of Dendrimers from Solutions onto Charged Surfaces, ACS Macro Letters 3(2) (2014) 180-184.

714 [69] V. Kuznetsov, K. Ottermann, N. Helfricht, D. Kunz, P. Loch, H. Kalo, J. Breu, G. Papastavrou,
715 Surface charge density and diffuse layer properties of highly defined 2:1 layered silicate platelets,
716 Colloid and Polymer Science 298(7) (2020) 907-920.
717 [70] M. Yanez Arteta, F. Eltes, R.A. Campbell, T. Nylander, Interactions of PAMAM Dendrimers
718 with SDS at the Solid–Liquid Interface, Langmuir 29(19) (2013) 5817-5831.

719